Towards Cosmological Simulations of Dark Matter on Quantum Computers

Philip Mocz[1] and Aaron Szasz[2,3]

[1]*Department of Astrophysical Sciences, Princeton University, 4 Ivy Lane, Princeton, NJ 08544, USA*
[2]*Perimeter Institute for Theoretical Physics, Waterloo, Ontario N2L 2Y5, Canada*
[3]*Materials Sciences Division, Lawrence Berkeley National Laboratory, Berkeley, CA 94720, USA*

ABSTRACT

State-of-the-art cosmological simulations on classical computers are limited by time, energy, and memory usage. Quantum computers can perform some calculations exponentially faster than classical computers, using exponentially less energy and memory, and may enable extremely large simulations that accurately capture the whole dynamic range of structure in the Universe within statistically representative cosmic volumes. However, not all computational tasks exhibit a 'quantum advantage'. Quantum circuits act linearly on quantum states, so nonlinearities (e.g. self-gravity in cosmological simulations) pose a significant challenge. Here we outline one potential approach to overcome this challenge and solve the (nonlinear) Schrödinger-Poisson equations for the evolution of self-gravitating dark matter, based on a hybrid quantum-classical variational algorithm framework (Lubasch et al. 2020). We demonstrate the method with a proof-of-concept mock quantum simulation, envisioning a future where quantum computers will one day lead simulations of dark matter.

1. INTRODUCTION

Quantum computers have enormous potential to exponentially speed up classical algorithms by leveraging the quantum mechanical features of *superposition* and *entanglement* (Feynman 1982). The elementary unit of a quantum computer is a *qubit* (a quantum version of the classical bit). Whereas n classical bits can encode 2^n integers, n qubits instead describe a vector space where each of these integers corresponds to one basis state. By acting on more general vectors (superpositions), operations can be performed in parallel on all basis states, with physical costs (energy) required for computation that only scale as n (Benenti & Strini 2008). Quantum computers, as they become a reality (Sevilla & Riedel 2020, e.g. Arute et al. 2019), will open new avenues for direct simulation of quantum systems (Kassal et al. 2008), factoring integers (Shor 1995), and solving systems of linear equations (Harrow et al. 2009), among

other applications (Abhijith et al. 2018). However, not all computational tasks are amenable to exponential speedup on a quantum computer. Limitations include (1) the unitarity and reversibility of quantum gates, (2) the impossibility of copying an arbitrary unknown quantum state (the *no-cloning* theorem; Park 1970), and (3) that output states are accessible only through measurement, making computational results probabilistic in nature. More broadly, computational complexity theory tells us that some problems are simply too hard to solve for any reasonable model of computation.

Whether and how, despite these limitations, *nonlinear* equations can be solved with exponential speedup using unitary (*linear*) quantum gates, remains an open research problem. Nonlinear products can be computed by preparing multiple copies of a quantum state (Leyton & Osborne 2008), so one could envision first preparing a state, then determining the evolved state at each timestep via measurement, then preparing further copies to use in the next timestep. But this approach would be far worse than a classical simulation, as determining an arbitrary wavefunction requires exponentially many measurements in the number of qubits and

Corresponding author: Philip Mocz
pmocz@astro.princeton.edu

retains statistical errors not present in classical computation. Additionally, preparing an arbitrary state is difficult (Aharonov & Ta-Shma 2003). Alternatively, the problem of measuring and preparing arbitrary states could be avoided by carrying out many copies of the time evolution from the initial state in parallel, but this would require exponentially many copies in the number of timesteps. Thus something beyond these naive approaches is needed. Despite recent progress on solving nonlinear equations by direct simulation (Liu et al. 2020; Lloyd et al. 2020), we focus instead on the use of variational quantum computing (VQC; Cerezo et al. 2020).

VQC finds the solution to a nonlinear equation using the key concept that the problem can be written as a function of variational parameters, and optimal parameters can be found by minimizing a cost function. The generally expensive-to-compute cost function is calculated on a quantum computer, while the parameter optimization is done classically; VQC is consequently a hybrid quantum-classical approach. A VQC method for solving nonlinear differential equations was outlined and demonstrated in Lubasch et al. (2020) with 2 qubits on the Noisy Intermediate-Scale Quantum (NISQ) IBM-Q device and with a 13 qubit mock simulation using matrix product states (Schollwöck 2011). The VQC framework has been considered for simulating nonlinear systems in quantum chemistry (Kreula et al. 2016), Navier-Stokes fluids (Griffin et al. 2020), and plasma physics (Dodin & Startsev 2020).

Nonlinear differential equations underlie simulations of cosmic structure formation, which would benefit from larger simulations. Galaxies form in the self-gravitating (nonlinear) potential wells of dark matter halos. A statistically representative volume of the Universe requires Gigaparsec box sizes, while galaxies are kiloparsec-scale: $10^6 \times$ smaller in linear dimension (Potter et al. 2017). Halos span from massive 10^{14} $M_\odot$ structures to potentially Earth-mass subhalos: 19 orders of magnitude (Bringmann 2009). The small-scale distribution of dark matter may highlight interesting additional physics in the nature of dark matter (e.g. self-interactions) but is inextricably linked to larger scales (Bullock & Boylan-Kolchin 2017). This huge dynamic range is far from achievable by today's classical supercomputers (Genel et al. 2014; Garrison et al. 2018), hence technological innovation that allows for larger simulations is essential.

This manuscript's aim is to begin bridging emerging quantum computing technology and applications to cosmological simulations. We first describe the physical system of interest (§ 2) and a classical spectral solver (§ 3). We present a high-level overview of a VQC algorithm (§ 4) that in principle would exponentially speed up cosmological simulations of dark matter, along with a proof-of-concept mock simulation (§ 5). Finally, we discuss the method's advantages and limitations and offer some perspective for the near future (§ 6).

2. SELF-GRAVITATING DARK MATTER IN AN EXPANDING UNIVERSE

Consider the evolution of a (non-relativistic) dark matter scalar field in an expanding universe. In dimensionless form, the evolution of the complex wavefunction ψ describing the dark matter as a function of time t is given by the Schrödinger-Poisson equations:

$$i\frac{\partial}{\partial t}\psi = -\frac{\nabla^2}{2}\psi + aV\psi \tag{1}$$

$$\nabla^2 V = |\psi|^2 - 1 \tag{2}$$

where $a \equiv a(t)$ is the prescribed cosmic scale factor that encodes underlying cosmological expansion. ψ is normalized over the volume $\mathcal{V}$ such that $\frac{1}{\mathcal{V}} \int |\psi|^2 \, d\mathcal{V} = 1$.

The equations are applicable to a range of dark matter models, including ultra-light boson dark matter ('fuzzy dark matter'; Hu et al. 2000; Schive et al. 2014; Hui et al. 2017; Mocz et al. 2017) as well as standard collisionless cold dark matter (CDM) in the limit that the particle mass tends to infinity. In the large mass limit, the Schrödinger-Poisson equations approximate the Vlasov-Poisson equations (Widrow & Kaiser 1993; Kopp et al. 2017; Mocz et al. 2018), which are the more commonly solved equations in CDM simulations. The idea of evolving CDM dynamics via this 'Schrödinger-Vlasov correspondence' (Mocz et al. 2018) has been proposed since Widrow & Kaiser (1993), although in practice simulations on classical computers commonly solve the Vlasov-Poisson equations directly via N-body methods (Boylan-Kolchin et al. 2009; Potter et al. 2017).

Our focus here is the Schrödinger-Poisson equations for quantum computer simulations because its form directly evolves a wavefunction, making it more more readily applicable to quantum simulation. We point out that the VQC method that we outline for solving the Schrödinger-Poisson equations in § 4.3 may generalized to other sets of nonlinear equations as well; the evolved quantity need not be a wavefunction but can be any smooth field. An advantage of working with the Schrödinger-Poisson equation as opposed to the Vlasov-Poisson equation, however, is that the solution is smooth in the former, whereas the the Vlasov-Poisson equation often exhibits singularities, caustics, and discontinuities.

Initial conditions representing the early Universe are typically set by sampling a random Gaussian field with
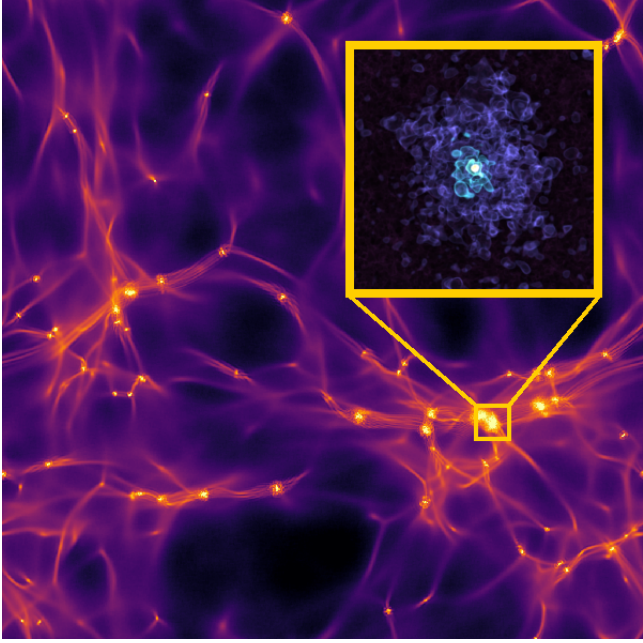
Figure 1. A simulated cosmological volume from Mocz et al. (2017) evolved by solving the Schrödinger-Poisson equations using the classical algorithm of § 3. Shown is the log of projected density. The inset highlights an individual dark matter halo and its small-scale features.

a prescribed power spectrum, and cosmological simulations may be evolved to the present day. A domain periodic in all spatial dimensions is commonly assumed. Of particular interest is the evolution of the dark matter density 1D power spectrum, which is compared against observationally inferred values in order to constrain cosmological models (Iršič et al. 2017; Planck Collaboration et al. 2018), as well as other global statistical properties such as the halo mass function or the subhalo abundance distribution (Boylan-Kolchin et al. 2009).

3. CLASSICAL ALGORITHM

The Schrödinger-Poisson equations (Eqns. (1) and (2)) may be solved with a classical spectral method, which consists of applying unitary operators, Fast Fourier Transforms (FFTs), and inverse FFTs (Mocz et al. 2017), and has been applied to cosmological simulations (Mocz et al. 2017, 2019, 2020).

Algorithm 1 shows the steps of the spectral method. The system state $\boldsymbol{\psi}$ is an array of N^3 grid elements and $\boldsymbol{k}$ is an array of corresponding wavenumbers in the spectral decomposition. The system is evolved for N_t timesteps. A '.' denotes an element-wise broadcast operator (e.g. used for multiplication or division).

Algorithm 1 Spectral algorithm (classical)

1: **for** $i = 1, \ldots, N_t$ **do**
2:      $\hat{\boldsymbol{\psi}} \leftarrow \text{FFT}(\boldsymbol{\psi})$
3:      $\hat{\boldsymbol{\psi}} \leftarrow \exp(-i\frac{\boldsymbol{k}^2}{2}\Delta t).*\hat{\boldsymbol{\psi}}$
4:      $\boldsymbol{\psi} \leftarrow \text{iFFT}(\hat{\boldsymbol{\psi}})$
5:      $\boldsymbol{\rho} \leftarrow |\boldsymbol{\psi}|^2$
6:      $\hat{\boldsymbol{V}} \leftarrow -\text{FFT}(\boldsymbol{\rho}-1)./\boldsymbol{k}^2$
7:      $\boldsymbol{V} \leftarrow \text{iFFT}(\hat{\boldsymbol{V}})$
8:      $\boldsymbol{\psi} \leftarrow \exp(-i\boldsymbol{V}\Delta t).*\boldsymbol{\psi}$

Given a resolution of N^3 grid elements and N_t timesteps, the method scales as $\mathcal{O}(N_t N^3 \log(N^3))$. The method has second-order accuracy in time (the error is due to the non-commutative nature of the kinetic and potential operators in the Schrödinger-Poisson equation); the time-scale to which Δt should be compared is $\hbar/(m|V_{\max}|)$ (Garny & Konstandin 2018). Being a spectral method, it has exponential convergence properties in space (as long as the maximal wavenumber is resolved). Time evolution using the spectral method is unconditionally stable both for constant V and for V given by Eqn. (2) (Garny & Konstandin 2018), a constraint which is independent of the spatial resolution. Thus N_t need not scale with N.

Fig. 1 shows an example of a simulated cosmological volume; shown is projected density ($|\psi|^2$) for a simulation using 1024^3 resolution elements (Mocz et al. 2017).

4. QUANTUM SIMULATION

4.1. *Basics: states and operators*

We first introduce quantum states and operators and discuss the concept of 'quantum advantage' over classical algorithms.

A quantum computer with n qubits encodes a quantum state $|\varphi\rangle$ that lives in an $N \equiv 2^n$-dimensional complex Hilbert space: $|\varphi\rangle = \sum_{l=0}^{N-1} c_l |l\rangle$, where the c_l are complex numbers satisfying the normalization condition $\sum_{l=0}^{N-1} |c_l|^2 = 1$. Each basis state $|l\rangle$ is specified by each of the n qubits being in the state $|0\rangle$ or the state $|1\rangle$, i.e. the 2^n basis states range from $|0\rangle \otimes \ldots |0\rangle \otimes |0\rangle$ to $|1\rangle \otimes \ldots |1\rangle \otimes |1\rangle$ (commonly notated as $|0\ldots0\rangle$ to $|1\ldots1\rangle$).

In the context of numerically solving the Schrödinger-Poisson equations, or any other differential equation, this allows for a much more efficient representation of a discretized function on $N = 2^n$ points. In the classical spectral method of § 3, the wavefunction at each timestep is represented as a length N vector, but as a quantum state it can be represented using just $n = \log_2(N)$ qubits. E.g., for a discretized function on the interval $[0, 1)$, the value of the function at location

$x \equiv \text{binary}(l) = \frac{1}{2} \sum_{j=0}^{n-1} l_j 2^{-j}$, with each l_j in $\{0, 1\}$, is the coefficient of the basis state $|l_0, \cdots, l_{n-1}\rangle$.

This more efficient representation of states can, for some problems, also lead to more efficient computations. Classically, even a simple operator like elementwise multiplication on a length-N vector must take time at least linear in N, while the same operator acting on the quantum state could potentially take time only linear/polynomial in n, i.e., an exponential speedup. However, some operators will still take time proportional to N, so it is essential to determine for a given problem whether an efficient implementation is indeed available.

One way of measuring the complexity of implementing an operation on a quantum computer is the minimal number of 1- and 2-site fundamental gates into which the operation can be decomposed; the particular fundamental gates that can be used vary depending on the particular hardware implementation, but gates that are commonly available include the Hadamard gate

$$H \equiv \frac{|0\rangle + |1\rangle}{\sqrt{2}} \langle 0| + \frac{|0\rangle - |1\rangle}{\sqrt{2}} \langle 1|, \qquad (3)$$

which implements a local change of basis on a qubit, phase-shift gates

$$R(\phi) \equiv |0\rangle\langle 0| + e^{i\phi}|1\rangle\langle 1| \qquad (4)$$

for some particular angles ϕ, and the two-qubit controlled-NOT gate,

$$\text{CNOT} \equiv |00\rangle\langle 00| + |01\rangle\langle 01| + |10\rangle\langle 11| + |11\rangle\langle 10|, \quad (5)$$

which creates entanglement between qubits. Two particular important phase shift gates are the S and T gates, with $\phi = \pi/2$ and $\pi/4$, respectively. Indeed, the gate set $\{H, S, T, \text{CNOT}\}$ is universal, meaning that any gate can be arbitrarily well-approximated by some combination of these gates (Bravyi & Kitaev 2005).

A quantum circuit to implement some operation (e.g. one timestep in a differential equation) is built from some number of layers of these gates applied to the n qubits encoding the state of the system; the number of layers is called the depth of the circuit. Since multiple gates within a single layer can be applied in parallel, the time to run a circuit scales with the depth, making the depth a good measure of computational complexity; another useful measure is the total number of gates, which is larger by a factor of at most n.

To demonstrate an exponential quantum speedup, we need not consider any particular fundamental gate set, since implementing a more general one-, two, or even three-qubit gate with a given accuracy will require a number of fundamental gates that does not scale with the system size. Thus it will be sufficient for our purposes to demonstrate that there are circuits with polynomial depth in the number of qubits, regardless of the gates that appear in the circuit. (If the hardware only allows gates between nearby qubits, an m-qubit gate may also require up to $\mathcal{O}(n^{m-1})$ swap gates to bring the qubits together, incurring an additional polynomial, but not an exponential, cost.)

4.2. Quantum simulation of a linear Schrödinger equation

Before considering the application of quantum simulation to the full Schrödinger-Poisson equations (Eqns. (1) and (2)), we first discuss the simpler case of the one-dimensional Schrödinger equation (Eqn. (1)) in a fixed potential V. As this is a linear equation, the quantum simulation can be performed by directly applying a quantum circuit; we follow the algorithm laid out in Benenti & Strini (2008). The method we describe here is similar to the classical algorithm and serves as a good introduction to quantum simulations. However, unlike the classical analog, it cannot be easily extended to nonlinear equations, for which an entirely different algorithm will be needed (VQC; § 4.3). The inclusion of the discussion of the linear solver here helps highlight the unique challenges when it comes to designing quantum algorithms.

To represent the wavefunction $\psi(x, t)$ on the domain $[0, L]$ as a quantum state, we first discretize the spatial domain into $N = 2^n$ equally spaced points $x_l \equiv l\Delta x$ for $l = 0, \cdots, N-1$ (so $\Delta x \equiv L/N$), then set the value of ψ at the point x_l as the coefficient of basis state $|l\rangle$:

$$|\Psi\rangle = \frac{1}{\sqrt{N}} \sum_{l=0}^{N-1} \psi(x_l, t)|l\rangle. \qquad (6)$$

The normalization factor $N^{-1/2}$ corrects for the fact that $\psi(x, t)$ is normalized to the system volume, L, while the quantum state is necessarily normalized to 1.

To perform one timestep, we follow essentially the same algorithm as in the pseudocode of § 3: Fourier transform, multiply by $\exp(-ik^2\Delta t/2)$, inverse Fourier transform, and multiply by $\exp(-iV(x)\Delta t)$. In other words, the algorithm must, for each timestep, compute

$$|\Psi\rangle \leftarrow e^{-iV\Delta t}\text{iQFT}\left(e^{-i\frac{k^2}{2}\Delta t}\text{QFT}\left(|\Psi\rangle\right)\right) \qquad (7)$$

Each of these operations (assuming a reasonable potential V) can indeed be efficiently implemented, as measured by the required circuit depth.

The 'QFT' in Eqn. (7) is the well-known Quantum Fourier Transform (Coppersmith 2002), which can be

performed efficiently (Hales & Hallgren 2000) and maps:

$$\sum_{k=0}^{N-1} f(k)|k\rangle \leftarrow \sum_{l=0}^{N-1} \hat{f}(l)|l\rangle \qquad (8)$$

where

$$\hat{f}(l) \equiv \frac{1}{\sqrt{N}} \sum_{k=0}^{N-1} e^{2\pi i k l/N} f(k) \qquad (9)$$

are the discrete Fourier Transform coefficients. The number of gates in the QFT algorithm scales as $\mathcal{O}(n^2)$, in contrast with the $\mathcal{O}(2^n n)$ classical FFT.

The other basic operation required is multiplication by a function,

$$|x\rangle \leftarrow e^{if(x)}|x\rangle. \qquad (10)$$

In the important case where $f(x)$ is a polynomial of degree m, this can be implemented with n^m gates, each acting on m qubits, as outlined in Benenti & Strini (2008). Consider as an illustrative example the harmonic oscillator potential $V(x) = x^2$. Write the discretized variable x via binary expansion as $(\Delta x/2)\sum_{j=0}^{n-1} l_j 2^{-j}$, where k_j represents the j qubit state. Then $x^2 = (\Delta x/2)^2 \sum_{i,j=0}^{n-1} l_i l_j 2^{-(i+j)}$ and

$$e^{-iV(x)\Delta t} = \prod_{i,j=0}^{n-1} \exp\left(-i\Delta t \left(\frac{\Delta x}{2}\right)^2 l_i l_j 2^{-(i+j)}\right). \qquad (11)$$

Each of the n^2 factors is implemented by a gate acting only on qubits i and j. Note that in combination with the QFT, the exact same method applies to the kinetic operator $f(k) \propto k^2$.

The overall computation time for each timestep, assuming $e^{-iV(x)\Delta t}$ has an efficient implementation, is poly(n), which is indeed an exponential speedup compared with the classical spectral method. As numerical stability does not require the number of timesteps to scale with spatial resolution, this exponential speedup also applies to the full computation of the final state from the initial one. There remains the question of how to efficiently extract physical observables from the final state in, a discussion which we postpone to § 4.4.

4.3. Cosmological (nonlinear) simulations with quantum-classical hybrid approach

We now consider a quantum algorithm for solving the full (nonlinear) Schrödinger-Poisson system.

It is not possible to straightforwardly adapt the linear quantum simulation algorithm of § 4.2 to these nonlinear equations. One point of difficulty lies in the calculation of the density $|\psi|^2$, needed to obtain the self-potential. Unitary operators are unable to simply square coefficients of a quantum state, and the *no-cloning* theorem

$\{\cdot\}$ repeated $d = 3$ times
($\ell = 0, 1, 2$)
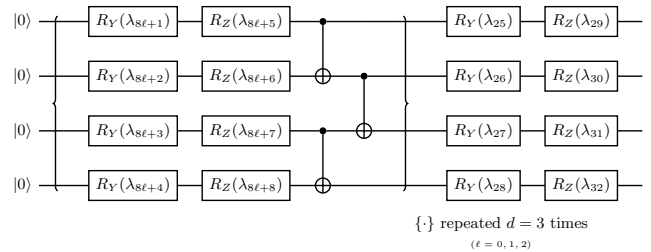
Figure 2. Example of a quantum variational ansatz $U_j(\boldsymbol{\lambda})$ that uses $\mathcal{O}(\text{poly}(n))$ parameters $\boldsymbol{\lambda}$ to represent a solution field of size 2^n. Here $R_Y(\lambda) = \cos(\lambda)\text{Id} + i\sin(\lambda)\sigma_y$ and superposes $|0\rangle$ and $|1\rangle$; $R_Z(\lambda) = \cos(\lambda)\text{Id} + i\sin(\lambda)\sigma_z$ and is a phase rotation, equivalent to $R(-2\lambda)$ for R defined in Eqn. (4); and each two-qubit gate appearing in the third layer is CNOT defined in Eqn. (5). The variational circuit has $(2d + 2)n$ parameters, where d is the circuit depth, and d must be at least $\mathcal{O}(n)$ to represent a generic state.

means it is impossible to clone the state $|\Psi\rangle$. Instead, we consider applying the hybrid quantum-classical VQC algorithm of Lubasch et al. (2020).

In VQC, any state $|\varphi\rangle$ is given by a *quantum circuit ansatz* $U(\boldsymbol{\lambda})$ that depends on some list of classical parameters $\boldsymbol{\lambda}$, $|\varphi\rangle \equiv |\varphi(\boldsymbol{\lambda})\rangle = U(\boldsymbol{\lambda})|0\rangle^{\otimes n}$; one commonly used hardware-efficient ansatz (O'Malley et al. 2016; Shen et al. 2017; Kandala et al. 2017) for the circuit U is shown in Fig. 2. It is easy to obtain multiple copies of any given ansatz state: the parameters $\boldsymbol{\lambda}$ are classical and can simply be stored and then used as many times as needed to generate more copies. It is also easy to generate the complex conjugate $|\varphi^*\rangle$ when the parameters for $|\varphi\rangle$ are known—for example, in the ansatz from Fig. 2, one simply multiplies the classical parameters for all R_Z gates by -1.

To simulate the Schrödinger-Poisson system, the wavefunction ψ and potential V at each timestep are each given by just such an ansatz state, $|\Psi(\boldsymbol{\lambda})\rangle$ and $|V(\tilde{\boldsymbol{\lambda}})\rangle$ respectively. The computational task in each timestep is to first find a new set of parameters $\tilde{\boldsymbol{\lambda}}$ that give the best approximation to the self-potential due to the current wavefunction, then to find a new set of $\boldsymbol{\lambda}$ that give the best approximation to the new state after the timestep. Each of these optimizations is performed classically, for example using standard approaches such as Nelder-Mead, quasi-Newton methods or others, (Spall 1998), with the cost function computed using quantum circuits; it is important to note that each cost function involves a measurement of the quantum state, and thus for each set of classical parameters it must be evaluated a number of times. Also note that because the potential is real-valued, we may remove all R_Z gates from the

variational circuit for $|V\rangle$. The algorithm is summarized in Algorithm 2.

Algorithm 2 Quantum VQC Algorithm

1: **for** $i = 1, \ldots, N_t$ **do**
2:     **while** $\{\tilde{\boldsymbol{\lambda}}_i, \tilde{\lambda}_V\}$ not converged **do**
3:         $|\Psi\rangle, |\Psi^*\rangle \leftarrow \boldsymbol{\lambda}_{i-1}; \; |V\rangle \leftarrow \tilde{\boldsymbol{\lambda}}_i$
4:         Cost $= ||\,(|\boldsymbol{\psi}|^2 - 1) - \tilde{\lambda}_V \nabla^2 \boldsymbol{V}\,||^2$
5:     **while** $\boldsymbol{\lambda}_i$ not converged **do**
6:         $|\Psi\rangle \leftarrow \boldsymbol{\lambda}_{i-1}; \; |V\rangle \leftarrow \tilde{\boldsymbol{\lambda}}_i; \; |\psi'\rangle \leftarrow \boldsymbol{\lambda}_i$
7:         Cost $= ||\,(\boldsymbol{\psi}' - \boldsymbol{\psi}) + i\Delta t(\tilde{\lambda}_V \boldsymbol{V} + \nabla^2)\boldsymbol{\psi}'\,||^2$

At each timestep we first find the variational parameters $\tilde{\boldsymbol{\lambda}}$ for the state representing the potential, $|V\rangle$. We also need an additional variational parameter $\tilde{\lambda}_V$ that normalizes $|V\rangle$ to the physical value of the potential. (We present the cost functions in terms of the vectors represented by the quantum states, rather than the states themselves, but will clarify below exactly how the cost functions can be computed from the states in practice.) If the ansatz for $|V\rangle$ is fully general, then the cost function will be minimized at 0 when the Poisson equation (Eqn. 2) is solved exactly. Once the new parameters for the potential have been determined, we complete the timestep by optimizing the new parameters for $|\Psi\rangle$, using the just-computed potential in the cost function.

What remains to be discussed is the computation of cost functions, lines 4 and 7 of Algorithm 2. For each cost function, we break it up into many terms, each of which is a vector product, and then for each term design a quantum circuit whose average output over many runs will give the value of that vector product (with an additional factor that can be included classically at the end).

The first step is to replace the spatial derivatives ∇^2 of $\boldsymbol{V}$ and $\boldsymbol{\psi}'$ by discretized derivatives. In one dimension, $\nabla^2 \boldsymbol{\psi}'$ for example becomes $\left(\boldsymbol{\psi}'_{-1} - 2\boldsymbol{\psi}' + \boldsymbol{\psi}'_{+1}\right)/(\Delta x)^2$, where $\boldsymbol{\psi}'_{\pm 1} = \boldsymbol{\psi}'(x \pm \Delta x)$; the quantum state for $\boldsymbol{\psi}'_{\pm 1}$ is $|\Psi'_{\pm 1}\rangle = \frac{1}{\sqrt{N}} \sum_l \psi'(x_l)|l \mp 1\rangle$. An explicit shift circuit to compute, e.g., $|\Psi_{+1}\rangle$ from $|\Psi\rangle$ by shifting each coefficient to the previous basis state is given by Fig. S2 of Lubasch et al. (2020) with the unseen control qubit set to $|1\rangle$. The resulting cost function for the potential becomes $||\,(|\boldsymbol{\psi}|^2 - 1) - (\tilde{\lambda}_V/\Delta x^2)(\boldsymbol{V}_{-1} - 2\boldsymbol{V} + \boldsymbol{V}_{+1})\,||^2$, with the cost function for $\boldsymbol{\psi}'$ likewise modified.

We can now divide the terms appearing in the two cost functions into four types: the four-state product $|\boldsymbol{\psi}|^2 \cdot |\boldsymbol{\psi}|^2$; the three-state products $|\boldsymbol{\psi}|^2 \cdot \boldsymbol{V}$ and $|\boldsymbol{\psi}|^2 \cdot \boldsymbol{V}_{\pm 1}$; the single-vector sums $\mathbf{1} \cdot \boldsymbol{V}$ and $\mathbf{1} \cdot \boldsymbol{V}_{\pm 1}$; and many two-state products, e.g. $\boldsymbol{\psi}^* \cdot \boldsymbol{\psi}'$.

A circuit for $|\boldsymbol{\psi}|^2 \cdot |\boldsymbol{\psi}|^2$ is given explicitly in Lubasch et al. (2020), Figs. 1(a) and 2(a). Likewise the three-

state products can be computed using the circuits in Figs. 1(a) and 2(b) of the same reference, with the box labeled "V" in 2(b) being the variational circuit for $|V\rangle$ followed by, for the $\boldsymbol{V}_{\pm 1}$ terms, the appropriate shift circuit as discussed above. Note that the results of these circuits must also be multiplied by scalar factors, for example N^2 for $|\boldsymbol{\psi}|^2 \cdot |\boldsymbol{\psi}|^2$, to get the final cost function contributions.

Two-vector products like $\boldsymbol{\psi}^* \cdot \boldsymbol{\psi}'$ are found using the state overlap $\langle \Psi | \Psi' \rangle$. However, some care is required because algorithms like the well-known swap test circuit (Buhrman et al. 2001) for state overlap return the magnitude of the overlap, but in our case we need $\langle \Psi | \Psi' \rangle + \langle \Psi' | \Psi \rangle$ which in general is different from $|\langle \Psi | \Psi' \rangle| + |\langle \Psi' | \Psi \rangle|$. Fortunately, since $\langle \Psi | \Psi' \rangle + \langle \Psi' | \Psi \rangle$ is real, it is sufficient to find the real part of $\langle \Psi | \Psi' \rangle$. This can be computed using the Hadamard test circuit (Nielsen & Chuang 2002), which for a state $|\varphi\rangle$ and unitary operator U returns the real part of $\langle \varphi | U | \varphi \rangle$. In our case, for $|\varphi\rangle$ we use the n-qubit state $|\mathbf{0}\rangle$ and for the unitary we use $U(\boldsymbol{\lambda})^\dagger U(\boldsymbol{\lambda}')$, where $U(\boldsymbol{\lambda})$ is the variational circuit for $|\Psi\rangle$ and $U(\boldsymbol{\lambda}')$ for $|\Psi'\rangle$; note that $U^\dagger$ can be found by running the circuit for U in reverse, taking the Hermitian conjugate of each R_Z and R_Y gate. This same circuit is also given in Lubasch et al. (2020), Figs. 1(a) and S3(a). With this approach, all terms in the cost function for the wavefunction can be organized into complex conjugate pairs, and the total contribution of the pair can be computed by finding the real part of one of the two terms; again, a scalar multiple is also needed for each term.

Finally, the single-vector sums can also be found by the overlap of two states. In this case, the vector $\mathbf{1}$ can be represented by the quantum state $(H|0\rangle)^{\otimes n}$, which has all coefficients equal to $2^{-n/2}$, along with a scalar multiple of $\sqrt{N}$ as a correction. Here, since $\boldsymbol{V}$ is real, finding the magnitude of the overlap for each term is sufficient, so the swap test can be used rather than the more general Hadamard test approach outlined above.

We thus can construct an explicit circuit for each term in the cost functions, and the value of the term is given by the average of a measurement made after each of many runs of the circuit. For M circuit evaluations, the error scales as $M^{-1/2}$; in the large-n limit, the relative error also grows linearly in N, which would seem to require an exponentially large number of samples. Fortunately, this scaling only holds once n is large enough to converge all spatial features, so in the regime of physical interest it does not present a problem (Lubasch et al. 2020).

This variational quantum algorithm gives an exponential speedup over classical methods. This is true for each

timestep, since the cost functions are evaluated by circuits with depth polynomial in n, and, as just noted above, the number of circuit evaluations M needed for converged measurement statistics for the cost functions only scales with n once n is large enough to resolve all features of the solution (Lubasch et al. 2020). Furthermore, with a good choice of optimization algorithm, it may not be necessary to converge the measurement statistics for each set of parameters (Sweke et al. 2020; Kübler et al. 2020). The last consideration for the cost of each individual timestep is the number of iterations needed to converge the classical optimization of the parameters. While some variational quantum algorithms suffer from the barren plateau problem (Cerezo et al. 2020), leading to an exponential number of iterations, this should not occur when the optimization is initialized close to the solution, which is the case in each timestep because we start with the parameters from the previous step and time evolution is continuous. Consequently, we expect that each timestep has total cost poly(n). Finally, for time-stepping we use a first-order implicit Euler method, so that numerical stability does not require the number of timesteps to scale with spatial resolution. As the actual time evolution produced by the simulation is the same as in the classical case, that the number of timesteps also need not scale with spatial resolution to achieve a numerically accurate solution carries over to the quantum simulation. As a result, the full simulation is also exponentially faster than for classical methods.

To conclude this section, we offer some important notes: (1) We use a second-order discretization for the Laplacian operator, and a first-order implicit Euler method for timestepping, but higher-order schemes are possible. (2) More efficient circuits for certain cost functions are possible. There has been some recent progress in using machine learning to optimize quantum circuits, including for computing overlaps (Cincio et al. 2018). (3) As noted above, when optimizing the cost functions, in practice it may not be necessary to converge measurement statistics for each value of $\boldsymbol{\lambda}$ or $\tilde{\boldsymbol{\lambda}}$. As demonstrated in Sweke et al. (2020) and Kübler et al. (2020), instead one can make only a small number of measurements for each term and use stochastic gradient descent, which provides a substantial speedup.

4.4. *Efficient computation of observables*

One major challenge in quantum computing is extracting useful information at the end of a simulation. In a classical calculation, the full state with $N = 2^n$ coefficients is known and can be used for further computations, for example of expectation values and other physical observables. The output of a quantum circuit,

however, is much less accessible. Measuring each qubit will return one of the 2^n basis states, and running the circuit and measuring its output many times will then give an approximate probability distribution over the basis states, in other words an approximation to $|\psi|^2$. This is, however, not practical. If any extensive fraction of the basis states have a non-negligible weight, it will require exponentially many measurements to extract a reasonable approximation, entirely defeating the purpose of using a quantum simulation in the first place. One could sample a much coarser grid, so that measurement statistics converge with a reasonable number of samples; this, however, loses important information contained in the final wavefunction. Alternatively, in the case of the variational algorithm, the exact state could in principle be reconstructed classically from the parameters at any given timestep. While using this approach to find the full final state after completing the variational quantum simulation would still be faster than performing a classical simulation, and depending on the output state could be more efficient than sampling many copies of the quantum state, it still incurs an exponential cost in n and hence is not practical if n is large enough that a quantum simulation is useful in the first place.

A better approach is to directly consider the quantities of physical interest extractable from the wavefunction, and to use quantum circuits that, with the final wavefunction as input, end with a measurement on just one or a few qubits that will give the desired quantity. Specializing to the dark matter simulations we discuss here, one particularly important quantity that can be compared with observational data is the power spectrum, i.e. the Fourier transform of ψ as a function only of the radial component of $\boldsymbol{k}$. While this still consists of $\mathcal{O}(2^n)$ numbers and hence is not efficiently measurable, moments of the power spectrum are easily accessible.

As discussed in § 4.3, there are efficient quantum circuits to compute products of wavefunctions, and these can be used to compute expectation values. The other key is that there are efficient quantum circuits to prepare states representing any polynomial: a polynomial of degree m can be represented exactly as a matrix product state with bond dimension $m + 1$ (Oseledets 2013), which can be converted into a low-depth quantum circuit (Lubasch et al. 2020) By using the product circuit with the state representing x^m, one copy of $|\Psi\rangle$, and one copy of $|\Psi^*\rangle$, the resulting measurements average to $\langle x^m \rangle$. This allows efficient computation of any moment $\langle x^l y^m z^p \rangle$. Moments of the power spectrum can be similarly obtained by first applying the QFT to both $|\Psi\rangle$ and $|\Psi^*\rangle$, in which case one would instead get $\langle k_x^l k_y^m k_z^p \rangle$.

Other observables may be efficiently computable using techniques from machine learning (Kiani et al. 2020).

Computation of observables in this manner is substantially faster using a variational method as in § 4.3 rather than a direct simulation as in § 4.2. In the former case, one need only run one copy of the low-depth variational circuit for the state in order to measure it, while in the latter case one must run the full simulation each time. This is one reason to consider using a variational method even if direct simulation is possible. Another, related benefit to using the variational approach is that the variational parameters can be stored classically not just for the final state, but indeed at each timestep, with relatively little memory, namely $N_t \text{poly}(n)$. Then observables can later be efficiently calculated for the state at any intermediate timestep, just as for the final state.

5. MOCK QUANTUM SIMULATION

We perform a mock simulation of the quantum Algorithm 2 (§ 4.3) where we simulate the entire quantum state on a classical computer and apply the quantum circuit in each step as a matrix multiplication. We consider the 1D Schrödinger-Poisson system on the domain $[0, 8]$ with initial condition $\psi(x, 0) = \sqrt{1 + 0.6 \sin(\pi x/4)}$ and evolve it until $t = 3$. In this simple problem, the overdensity in the initial condition collapses due to self-gravity and then splits into two during this time interval.

Fig. 3 shows the results of the simulation for $n = 2, 3, 4, 5, 6$ qubits, and an error analysis of numerical convergence to the classical reference solution carried out on an $N = 256$ grid. Note that we do not simulate the effect of measurement statistics, either in computing cost functions or in representing the final state; rather, we make use of our classical access to the full wavefunction.

A quasi-Newton (derivative-free) algorithm was used for minimization, and the quantum variational ansatz was taken to be of form Fig. 2 with depth $d = n - 1$. We have not optimized the choice of minimization algorithm or the form of the variational ansatz for our proof-of-concept demonstration, although our choice works reasonably well.

Different types of noise affect a quantum calculation, for which noise-resilient techniques are being developed (Fontana et al. 2020). We do not consider full hardware and measurement noise, but investigate the effect of adding random Gaussian errors to the variational parameters ($\lambda \leftarrow \lambda + \delta\lambda$) after each timestep to examine how errors may propagate during the nonlinear time evolution. Our simulations are robust to perturbations with $\delta\lambda \lesssim \mathcal{O}(10^{-5})$ (Fig. 3).

6. FUTURE PROSPECTS AND CONCLUDING REMARKS
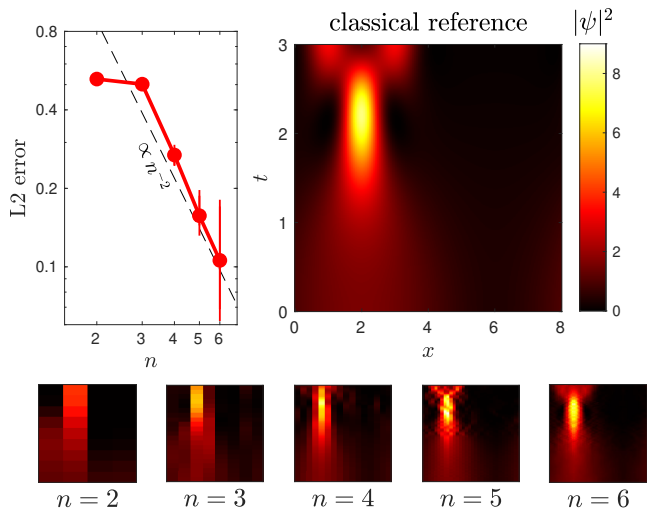
Figure 3. Proof-of-concept mock simulations of the quantum algorithm for the nonlinear 1D Schrödinger-Poisson system with $n = 2, 3, 4, 5, 6$ qubits and a reference solution used to demonstrate numerical convergence. Error bars show one standard deviation for 20 samples with $\mathcal{O}(10^{-5})$ perturbations to variational parameters at each timestep.

Emerging quantum computing technology has the potential to revolutionize cosmological simulations. Historically, simulation size has grown exponentially with time following Moore's Law (Fig. 1 of Genel et al. 2014). Quantum hardware may allow for even faster growth, or at least avoid exponentially growing energy costs.

We have outlined a VQC algorithm for efficiently evolving the *nonlinear* Schrödinger-Poisson equations for the cosmological simulation of dark matter, as well as a quantum algorithm for simulating *linear* Schrödinger systems which also has applications to certain problems in astrophysics (Lancaster et al. 2020). Both algorithms ($\mathcal{O}(N_t \text{poly}(n))$) offer an exponential speedup over classical simulations ($\mathcal{O}(N_t 2^n n)$). Physically relevant observables can be efficiently computed in the quantum simulation and compared against astrophysical observations. The VQC method may be generalizable to other sets of differential equations as well.

Our proof-of-concept mock simulation for nonlinear problems demonstrates that the quantum algorithm works in principle. In practice, current technology is limited by high error rates in two-qubit gates and fast loss of coherence due to interactions with the environment, making the algorithms inaccessible for the time being. However, with limited-depth circuits, our algorithm may become feasible even before the advent of fully error-corrected quantum computation.

Further improvements are certainly possible, including optimized choices for the quantum variational ansatz

and minimization algorithm, as well as more efficient circuits for computing the cost functions. A more exotic possibility is that of a direct, rather than variational, quantum algorithm for the simulation of the Schrödinger-Poisson equations. The equations preserve information and are reversible, so if any nonlinear system can be directly simulated, it is a strong candidate.

REFERENCES

Abhijith, J., Adedoyin, A., Ambrosiano, J., et al. 2018, arXiv e-prints, arXiv:1804.03719. https://arxiv.org/abs/1804.03719

Aharonov, D., & Ta-Shma, A. 2003, in Proceedings of the thirty-fifth annual ACM symposium on Theory of computing, 20–29

Arute, F., Arya, K., Babbush, R., et al. 2019, Nat, 574, 505, doi: 10.1038/s41586-019-1666-5

Benenti, G., & Strini, G. 2008, American Journal of Physics, 76, 657, doi: 10.1119/1.2894532

Boylan-Kolchin, M., Springel, V., White, S. D. M., Jenkins, A., & Lemson, G. 2009, MNRAS, 398, 1150, doi: 10.1111/j.1365-2966.2009.15191.x

Bravyi, S., & Kitaev, A. 2005, Physical Review A, 71, 022316

Bringmann, T. 2009, New Journal of Physics, 11, 105027, doi: 10.1088/1367-2630/11/10/105027

Buhrman, H., Cleve, R., Watrous, J., & de Wolf, R. 2001, Phys. Rev. Lett., 87, 167902, doi: 10.1103/PhysRevLett.87.167902

Bullock, J. S., & Boylan-Kolchin, M. 2017, ARA&A, 55, 343, doi: 10.1146/annurev-astro-091916-055313

Cerezo, M., Arrasmith, A., Babbush, R., et al. 2020, Variational Quantum Algorithms. https://arxiv.org/abs/2012.09265

Cincio, L., Subaşı, Y., Sornborger, A. T., & Coles, P. J. 2018, New Journal of Physics, 20, 113022, doi: 10.1088/1367-2630/aae94a

Coppersmith, D. 2002, arXiv e-prints, quant. https://arxiv.org/abs/quant-ph/0201067

Dodin, I. Y., & Startsev, E. A. 2020, arXiv e-prints, arXiv:2005.14369. https://arxiv.org/abs/2005.14369

Feynman, R. P. 1982, International Journal of Theoretical Physics, 21, 467, doi: 10.1007/BF02650179

Fontana, E., Fitzpatrick, N., Ramo, D. M., Duncan, R., & Rungger, I. 2020, arXiv preprint arXiv:2011.01125

Garny, M., & Konstandin, T. 2018, Journal of Cosmology and Astroparticle Physics, 2018, 009, doi: 10.1088/1475-7516/2018/01/009

Garrison, L. H., Eisenstein, D. J., Ferrer, D., et al. 2018, ApJS, 236, 43, doi: 10.3847/1538-4365/aabfd3

Genel, S., Vogelsberger, M., Springel, V., et al. 2014, MNRAS, 445, 175, doi: 10.1093/mnras/stu1654

Griffin, K., Jain, S., Flint, T., & Chan, W. 2020, Center for Turbulence Research Annual Research Briefs

Hales, L., & Hallgren, S. 2000, in Proceedings 41st Annual Symposium on Foundations of Computer Science, IEEE, 515–525

Harrow, A. W., Hassidim, A., & Lloyd, S. 2009, Phys. Rev. Lett., 103, 150502, doi: 10.1103/PhysRevLett.103.150502

Hu, W., Barkana, R., & Gruzinov, A. 2000, Phys. Rev. Lett., 85, 1158, doi: 10.1103/PhysRevLett.85.1158

Hui, L., Ostriker, J. P., Tremaine, S., & Witten, E. 2017, Phys. Rev. D, 95, 043541, doi: 10.1103/PhysRevD.95.043541

Iršič, V., Viel, M., Haehnelt, M. G., et al. 2017, Phys. Rev. D, 96, 023522, doi: 10.1103/PhysRevD.96.023522

Kandala, A., Mezzacapo, A., Temme, K., et al. 2017, Nat, 549, 242, doi: 10.1038/nature23879

Kassal, I., Jordan, S. P., Love, P. J., Mohseni, M., & Aspuru-Guzik, A. 2008, Proceedings of the National Academy of Science, 105, 18681, doi: 10.1073/pnas.0808245105

Kiani, B. T., Palma, G. D., Englund, D., et al. 2020, Quantum advantage for differential equation analysis. https://arxiv.org/abs/2010.15776

Kopp, M., Vattis, K., & Skordis, C. 2017, Phys. Rev. D, 96, 123532, doi: 10.1103/PhysRevD.96.123532

Kreula, J. M., Clark, S. R., & Jaksch, D. 2016, Scientific Reports, 6, 32940, doi: 10.1038/srep32940

Kübler, J. M., Arrasmith, A., Cincio, L., & Coles, P. J. 2020, Quantum, 4, 263, doi: 10.22331/q-2020-05-11-263

Lancaster, L., Giovanetti, C., Mocz, P., et al. 2020, Journal of Cosmology and Astroparticle Physics, 2020, 001, doi: 10.1088/1475-7516/2020/01/001

Leyton, S. K., & Osborne, T. J. 2008, arXiv e-prints, arXiv:0812.4423. https://arxiv.org/abs/0812.4423

Liu, J.-P., Øie Kolden, H., Krovi, H. K., et al. 2020, Efficient quantum algorithm for dissipative nonlinear differential equations. https://arxiv.org/abs/2011.03185

Lloyd, S., Palma, G. D., Gokler, C., et al. 2020, Quantum algorithm for nonlinear differential equations. https://arxiv.org/abs/2011.06571

Lubasch, M., Joo, J., Moinier, P., Kiffner, M., & Jaksch, D. 2020, Phys. Rev. A, 101, 010301, doi: 10.1103/PhysRevA.101.010301

Mocz, P., Lancaster, L., Fialkov, A., Becerra, F., & Chavanis, P.-H. 2018, Phys. Rev. D, 97, 083519, doi: 10.1103/PhysRevD.97.083519

Mocz, P., Vogelsberger, M., Robles, V. H., et al. 2017, MNRAS, 471, 4559, doi: 10.1093/mnras/stx1887

Mocz, P., Fialkov, A., Vogelsberger, M., et al. 2019, Phys. Rev. Lett., 123, 141301, doi: 10.1103/PhysRevLett.123.141301

—. 2020, MNRAS, 494, 2027, doi: 10.1093/mnras/staa738

Nielsen, M. A., & Chuang, I. 2002, Quantum computation and quantum information, American Association of Physics Teachers

Oseledets, I. V. 2013, Constructive Approximation, 37, 1, doi: 10.1007/s00365-012-9175-x

O'Malley, P. J., Babbush, R., Kivlichan, I. D., et al. 2016, Physical Review X, 6, 031007

Park, J. L. 1970, Foundations of Physics, 1, 23, doi: 10.1007/BF00708652

Planck Collaboration, Aghanim, N., Akrami, Y., et al. 2018, arXiv e-prints, arXiv:1807.06209. https://arxiv.org/abs/1807.06209

Potter, D., Stadel, J., & Teyssier, R. 2017, Computational Astrophysics and Cosmology, 4, 2, doi: 10.1186/s40668-017-0021-1

Schive, H.-Y., Chiueh, T., & Broadhurst, T. 2014, Nature Physics, 10, 496, doi: 10.1038/nphys2996

Schollwöck, U. 2011, Annals of Physics, 326, 96 , doi: https://doi.org/10.1016/j.aop.2010.09.012

Sevilla, J., & Riedel, C. J. 2020, Forecasting timelines of quantum computing. https://arxiv.org/abs/2009.05045

Shen, Y., Zhang, X., Zhang, S., et al. 2017, Physical Review A, 95, 020501

Shor, P. W. 1995, arXiv e-prints, quant. https://arxiv.org/abs/quant-ph/9508027

Spall, J. C. 1998, Johns Hopkins apl technical digest, 19, 482

Sweke, R., Wilde, F., Meyer, J., et al. 2020, Quantum, 4, 314, doi: 10.22331/q-2020-08-31-314

Widrow, L. M., & Kaiser, N. 1993, ApJL, 416, L71, doi: 10.1086/187073